

Article

Synthesis of Graphene-Oxide-Decorated Porous ZnO Nanosheet Composites and Their Gas Sensing Properties

Jie Li ^{1,2}, Zhen Jin ^{1,2,*} , Yang Chao ², Aijing Wang ², Decai Wang ², Shaohua Chen ^{1,2} and Quan Qian ²¹ Anhui Advanced Building Materials Engineering Laboratory, Anhui JianZhu University, Hefei 230601, China² School of Materials and Chemical Engineering, Anhui JianZhu University, Hefei 230601, China

* Correspondence: ftbjin@hotmail.com

Abstract: In this work, graphene-oxide-decorated porous ZnO nanosheets were prepared using a hydrothermal method. The graphene oxide/porous ZnO nanosheet (GO/ZnO nanosheet) composites were characterized with SEM, HRTEM, XRD, Raman spectroscopy, XPS and BET. The results indicate that the ZnO nanosheets have a porous, single-crystal structure. Thin GO nanosheets closely cover the surface of porous ZnO nanosheets. The sensing performance of GO/ZnO nanosheet composites is investigated. At the optimized temperature of 300 °C, the GO/ZnO nanosheet composites exhibit a superior sensing performance in n-propanol detection. In a wide range of 5–200 ppm, the composites exhibit a linear response to n-propanol. Moreover, the sensing performance of the GO/ZnO nanosheet composites to n-propanol is largely higher than that to other VOC gases, indicating a high selectivity in n-propanol detection. This can be ascribed to the higher electron-separation efficiency and larger depletion layer brought by the modification of the GO on ZnO nanosheets. It is considered that the GO/ZnO nanosheet composites have a great application potential in n-propanol detection.

Keywords: graphene oxide; ZnO nanosheet; n-propanol; sensing property



Citation: Li, J.; Jin, Z.; Chao, Y.; Wang, A.; Wang, D.; Chen, S.; Qian, Q. Synthesis of Graphene-Oxide-Decorated Porous ZnO Nanosheet Composites and Their Gas Sensing Properties. *Chemosensors* **2023**, *11*, 65. <https://doi.org/10.3390/chemosensors11010065>

Academic Editor: Boris Lakard

Received: 3 November 2022

Revised: 4 January 2023

Accepted: 6 January 2023

Published: 13 January 2023



Copyright: © 2023 by the authors. Licensee MDPI, Basel, Switzerland. This article is an open access article distributed under the terms and conditions of the Creative Commons Attribution (CC BY) license (<https://creativecommons.org/licenses/by/4.0/>).

1. Introduction

The demand for accurate detection for volatile organic compounds (VOCs) is increasing alongside the development of industrialization [1,2]. Therefore, many methods have been developed for the efficient detection of VOCs. Among various techniques, metal oxide semiconductor (MOS) gas sensors with benefits including fast response, low energy consumption and compact size are widely used [3–5]. Among MOS materials, ZnO has attracted great attention in the field of gas detection due to its excellent electronic and photonic properties [6–9]. However, owing to the large resistance value and the aggregation during the process of detection, pure ZnO sensing materials always suffer imperfections such as poor sensitivity and selectivity in VOC detection [10–12]. Numerous efforts have been devoted to enhance the performance of ZnO sensing materials [13–15]. Composite ZnO with a secondary material is a rational method to enhanced its sensing property, since the composite materials always combines the advantages of each component [16,17]. Aubekerov et al. synthesized ZnFe₂O₄-modified ZnO nanowires, which show better sensitivity than pure ZnO nanowires in isopropyl alcohol detection [18]. Xu et al. reported Eu(III)-functionalized ZnO@MOF heterostructures with excellent selectivity and sensitivity for aldehyde detection [19]. Nevertheless, it is still a big challenge to obtain ZnO-based sensing materials with superior sensing performance.

Two-dimensional materials, such as graphene and graphene oxide (GO), have attracted much attention due to their unique structures and excellent physical and chemical properties [20,21]. The unique two-dimensional network of graphene facilitates the exposure of all carbon atoms to air, allowing the maximum contact with the target molecules [17,22]. Wu et al. [23] found that a graphene/ZnO composite with low resistance exhibits better gas-sensing performance. GO, with abundant oxygen-containing functional groups, has a

similar structure to graphene, and can also be used as an ideal modifier to ZnO [24,25]. GO can not only effectively prevent the aggregation of ZnO nanomaterials, but also improve the electrical conductivity of ZnO materials, thus enhancing the sensing performance of the composites [26,27]. Singh et al. [28] prepared GO/ZnO composites using a one-step method, and these composites could efficiently detect NH₃ (1 ppm), NO (5 ppm) and CO (22 ppm) gases. Although many reports mention GO-modified sensing materials, it is still a big challenge to promote their sensing performance.

As one of the most widely used chemical raw materials, n-propanol is used in various industries, such as preservatives, detergents, cosmetics and pharmaceuticals [29]. However, n-propanol does harm to human health, and is known as a toxic volatile organic compound (VOC). When the concentration of n-propanol exceeds 400 ppm, it may impair the upper respiratory tract, retina and optic nerve. Therefore, the high-performance detection of n-propanol has attracted great interest in recent years [30]. In this work, graphene-oxide-decorated porous single-crystalline ZnO nanosheet (GO/ZnO nanosheet) composites were synthesized using a hydrothermal method. In the composites, the ZnO nanosheets of hexagonal wurtzite are closely wrapped by GO lamellae, and this unique structure makes the GO/ZnO nanosheet composites exhibit a high response, excellent selectivity and stability in n-propanol detection. At the optimized temperature of 300 °C, the GO/ZnO nanosheet composites exhibit a linear response in n-propanol detection. The sensing performance of the GO/ZnO nanosheet composites to n-propanol is much higher than to other VOC gases. The sensing mechanism is also discussed. It is believed that the GO/ZnO nanosheet composites have great potential for practical usage.

2. Materials and Methods

2.1. Materials

Zinc acetate, urea, sodium nitrate, potassium permanganate, graphite powder and concentrated sulfuric acid of analytical grade were purchased from Sinopharm Chemical Reagent Co., Ltd. (Shanghai, China) and used without further purification. Deionized water was used in all experiments.

2.2. Preparation of GO and Porous Single-Crystal ZnO Nanosheet Composites

GO was prepared using the modified Hummer method using graphite, sodium nitrate, concentrated sulfuric acid and potassium permanganate as raw materials. Graphite powder (0.5 g) and concentrated sulfuric acid (23 mL) were added to a 250 mL three-necked round-bottomed flask. The flask was sealed and stirred in an ice bath continuously overnight. NaNO₃ (0.5 g) was quickly added into the mixture and KMnO₄ (3 g) was slowly added for 30 min. Then the mixture was transferred to a 35 °C water bath under vigorous stirring for 1 h. Deionized water (40 mL) was slowly added and the system was heated up to 90 °C and stirred continuously for 2 h. Then a mixture of deionized water (10 mL) and hydrogen peroxide (30%) (3 mL) was slowly added and stirred for a few minutes. GO was prepared by filtering and washing the solution until it was neutral. GO (20 mg) was dissolved in 1 mL deionized water and ultrasonicated to form a 20 g/L GO dispersion.

The GO dispersion was added to a mixture of zinc acetate (1 g), urea (3 g) and 40 mL deionized water in a conical flask under ultrasound for 30 min. The conical flask was tightly corked and heated in an oven at 100 °C for 6 h, and then cooled to room temperature. Then, the complexes of GO and ZnO precursor were prepared. The product was washed with deionized water and ethanol by centrifugation and dried at 60 °C for 24 h. Finally, the GO-modified porous single-crystal ZnO nanosheet composites were prepared after calcinating the obtained samples at 300 °C for 2 h in air.

2.3. Characterization

The morphologies and structure of the samples were examined using field emission scanning electron microscopy (FESEM, FEI Sirion-200, Eindhoven, Netherlands) at 5 kV of accelerating voltage, and high resolution transmission electron microscopy (HRTEM,

JEOL JEM-2010, Tokyo, Japan) at 200 kV of accelerating voltage. The crystal structure of the samples was determined using X-ray diffraction (XRD, Philips X' pert PRO, Amsterdam, Netherlands) with Cu K α radiation, $\lambda = 0.15418$ nm. The Raman spectroscopy was processed with a Raman spectrometer (inVia, Renishaw, 532 nm wavelength, Gloucestershire, UK). X-ray photoelectron spectra (XPS) were recorded on an AXIS ULTRADLD spectrometer (Manchester, UK), with monochromatized Al K α X-rays as the excitation source and C 1s chosen as the reference line. N₂ adsorption/desorption isotherm was carried out at 77 K using an Autosorb-1-C analyzer (Quantachrome Instruments, Boynton Beach, FL, USA), and the corresponding pore size distribution was derived from the adsorption branch of the isotherm using the BJH method.

2.4. Fabrication of the Gas Sensor and the Gas-Sensing Measurement System

An illustration of the operating procedure of the gas sensor and its measurement system is shown in Figure 1. Two gold electrodes with a distance of 10 mm were added onto a ceramic tube. Next, two pairs of gold wires were closely bonded to those two gold electrodes. Then, a nichrome wire (with a resistance of 30 Ω) was placed in the interior of the ceramic tube as a heating wire. For the fabrication of the gas sensor, the prepared GO/ZnO nanosheet composite and porous ZnO nanosheet powders were dispersed in ethanol solvent and directly coated on the surface of the ceramic tube and then dried naturally at room temperature. The final thickness of the sensing film of the GO/ZnO nanosheet composite and porous ZnO nanosheet were both approximately 200 μm .

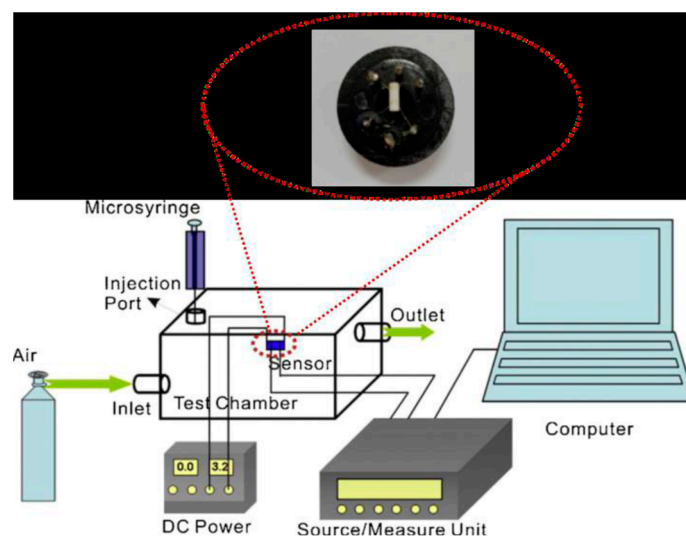


Figure 1. Schematic diagram of the experimental setup. The inset is the structure of the sensor.

The gas-sensing measurements were performed in a closed test chamber (1 L) equipped with an inlet and an outlet for gas. A Keithley 6487 Source/Measure Unit was used to record the change in current. When working, a constant voltage was applied onto the two gold electrodes between the sensing films, and the corresponding current was measured. In the typical gas-sensing test, certain amount of target gas was first collected from the headspace vapor of the organic solvent (e.g., methanol, ethanol, n-propanol, isopropanol, ammonia, methanal, benzene, water, etc., all of analytical grade), and then introduced into the test chamber using a microsyringe. The saturated vapor pressure of the organic vapor was recorded to calculate the concentration of the target gas under a standard atmospheric pressure. The injection rate of the target gas was about 1 mL/s. When the test was over, the target gas in the testing chamber was released by inputting fresh compressed air into the air bottle.

The response of the sensor is defined as:

$$\text{Response} = R_a/R_g = I_g/I_a \quad (1)$$

Here, R_a and R_g are the electric resistance of the sensor in air and the target gas, respectively. I_a and I_g are the electric current of the sensor in air and the target gas, respectively.

3. Results

3.1. Characterization

The porous ZnO nanosheets were first synthesized through a hydrothermal method, then the GO nanosheets were modified onto their surface. The morphologies of the porous ZnO nanosheets and the GO/porous ZnO nanosheet (GO/ZnO nanosheet) composites were investigated with SEM, and the results are shown in Figure 2. Figure 2a,b are the SEM images of the porous ZnO nanosheets at different magnifications. In these images, a great many nanosized pores can be clearly seen on the surface of the ZnO nanosheets. After the modification of GO nanosheets, from Figure 2c, it can be seen that the edges of the modified ZnO nanosheets are blurred. Furthermore, in the magnified image (Figure 2d), a thin and wrinkled structure can be observed on the surface of the nanosheets, indicating the successful modification of the lamellar GO on the porous ZnO nanosheets. The statistical distributions of the length and width of the GO/ZnO nanosheet composites are presented in Figure S1. The average length and width of the GO/ZnO nanosheet composites are 5.0 and 3.5 μm , respectively.

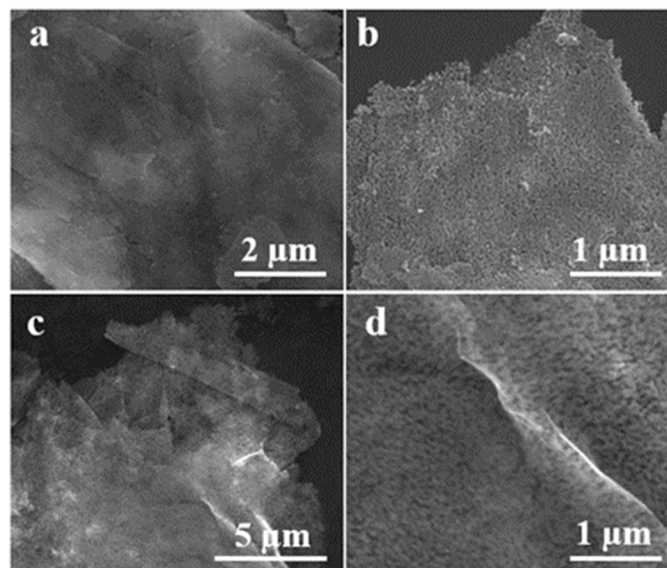


Figure 2. (a,b) SEM images of porous ZnO nanosheets, (c,d) GO/ZnO nanosheet composites, (b,d) are the magnification of (a,c), respectively.

Figure 3a,b are TEM images of the GO/ZnO nanosheets at different magnifications. It can be seen that the pores on the ZnO nanosheet are very rich, and the average diameter of the pores is about 30 nm. When looking closely at the surface of the ZnO nanosheets, it can be found that the ZnO nanosheet is covered with a thin layer of GO. In addition, at the edge of the ZnO nanosheet, the uncovered GO nanosheets also can be clearly observed. Figure 3c is the corresponding SAED pattern of the GO/ZnO nanosheet, which consists of well-ordered dots, indicating the single crystallinity of the porous ZnO nanosheets. The (112), (110) and (002) planes of wurtzite ZnO can also be indexed from the SAED pattern. Due to its small amount and poor crystallinity, the SAED pattern of GO cannot be observed. From the HRTEM image of GO/ZnO nanosheets (Figure 3d), it can be seen that the clear and coherent lattice fringes go throughout the nanosheet. The lattice spacing is 0.26 nm, which can be ascribed to the (002) plane of the hexagonal phase ZnO. Those results definitively prove the formation of the GO/ZnO nanosheet composites.

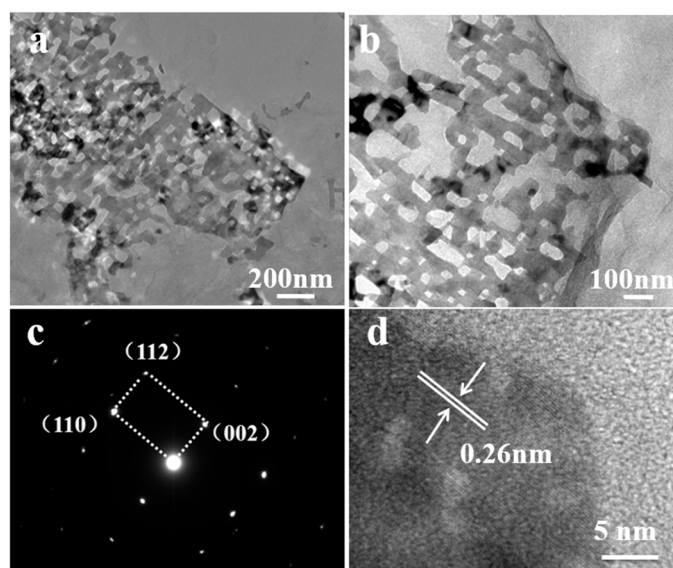


Figure 3. (a,b) TEM images of GO/ZnO nanosheets, (c) SAED pattern of the GO/ZnO nanosheets, (d) HRTEM image of GO/ZnO nanosheets.

The XRD patterns of pure porous ZnO nanosheets and GO/ZnO nanosheet composites are shown in Figure 4. All peaks in the porous ZnO nanosheets and GO/ZnO nanosheet composites correspond to the characteristic peaks of hexagonal wurtzite zinc oxide (JCPDS No. 36-1451), and no other peaks can be observed, indicating that there are no other impurities in the GO/ZnO nanosheet composites. The disappearance of the diffraction peak of GO in the composite material is due to its low amount and poor crystallinity.

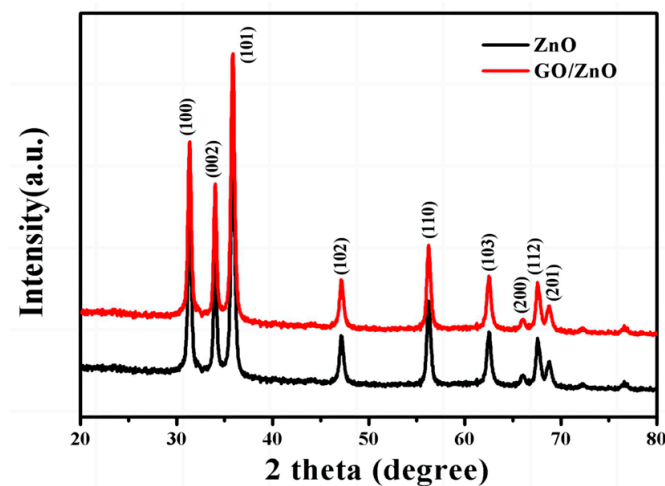


Figure 4. XRD patterns of the ZnO nanosheets and GO/ZnO nanosheet composites.

Raman spectroscopy is an effective method to characterize the structure of GO; thus, the GO nanosheets, porous single-crystal ZnO nanosheets and GO/ZnO nanosheet composites were characterized with Raman spectroscopy, and the results are presented in Figure 5. From the Raman spectra of the GO and GO/ZnO nanosheet composites, two obvious peaks at 1362 cm^{-1} and 1590 cm^{-1} can be observed, which correspond to the D and G bands of graphene, respectively. Furthermore, the Raman spectra of the GO/ZnO nanosheet composites also contain three small peaks at 322.2 , 432.3 and 562.2 cm^{-1} , which can also be observed in the Raman spectrum of the porous ZnO nanosheets. This result further confirms the combination of the ZnO nanosheets and GO.

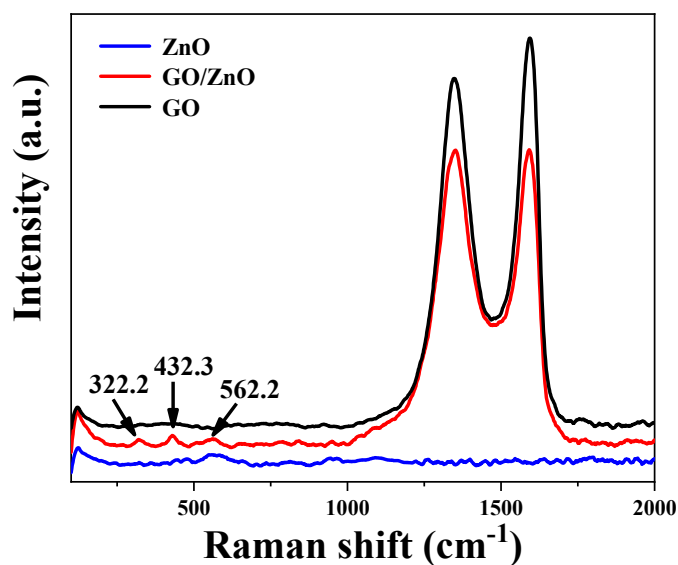


Figure 5. Raman spectra of pure GO, porous single-crystal ZnO nanosheets and GO/ZnO nanosheet composites.

The structure of GO/ZnO nanosheet composites was further investigated with XPS, and the results are shown in Figure 6. Figure 6a is the survey XPS spectrum of the composites, while Figure 6b presents the Zn 2p spectrum of the composites. The two characteristic peaks at 1044.6 and 1021.5 correspond to Zn 2p_{1/2} and Zn 2p_{3/2}, respectively, which are associated with the Zn-O bonding in ZnO. In Figure 6c, the C 1s peak of the GO/ZnO nanosheet composites can be deconvoluted into three peaks observed at 284.8, 286.2 and 288.7 eV, corresponding to functional groups C-C, C-O and C-COOH, respectively [21,31]. The O 1s spectrum (Figure 6d) can be deconvoluted into three peaks at 529.7, 531.2 and 532.5 eV, which correspond to the O²⁻ valance state (O-Zn bonding) in GO/ZnO nanosheet composites, oxygen vacancies and defects, and chemisorbed oxygen species, respectively [26,31]. The greater amount of oxygen vacancies and defects of the GO/ZnO nanosheet composites can help to trap electrons, improve the electron-hole recombination rate and keep a high carrier mobility, resulting in the enhanced sensing performance of the GO/ZnO nanosheet composites. The results are consistent with the sensing performance of the composites.

The N₂ adsorption/desorption isotherm of GO/ZnO nanosheet composites was studied and the result is presented in Figure 7. The N₂ adsorption/desorption isotherm of GO/ZnO nanosheet composites displays a type IV isotherm with an H3 hysteresis loop, which is typical of mesoporous materials. Figure 7b presents the pore size distribution of the composites. It can be seen that the average pore diameter is around 18.8 nm, which is consistent with the TEM result. The BET surface area of the GO/ZnO nanosheet composites is 25.1 m²g⁻¹, which is larger than that of the ZnO nanosheet (21.3 m²g⁻¹) [32]. The larger surface area and abundant pore structure of the GO/ZnO nanosheet composite make it a promising candidate for VOC detection.

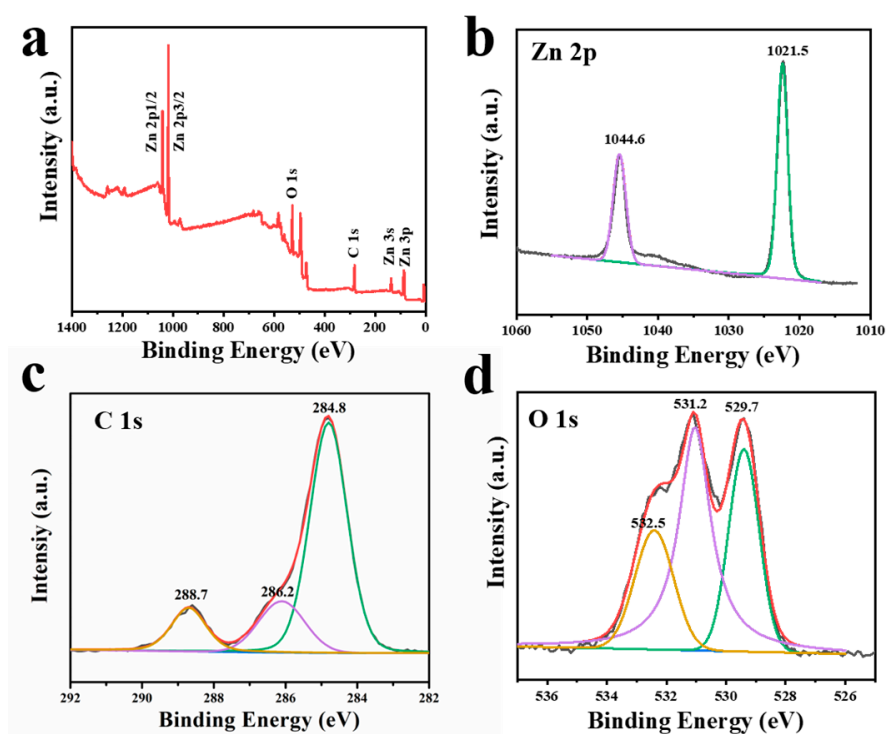


Figure 6. (a) Survey XPS spectrum of GO/ZnO nanosheet composites, and the corresponding elements' high-resolution XPS spectra: (b) Zn 2p, the purple line corresponds to Zn 2p_{1/2} and the green line corresponds to 2p_{3/2}, respectively, (c) C 1s, the green, purple and yellow line correspond to functional groups C-C, C-O and C-COOH, respectively, (d) O 1s, the green, purple and yellow line correspond to O-Zn bonding, oxygen vacancies and defects, and chemisorbed oxygen species, respectively.

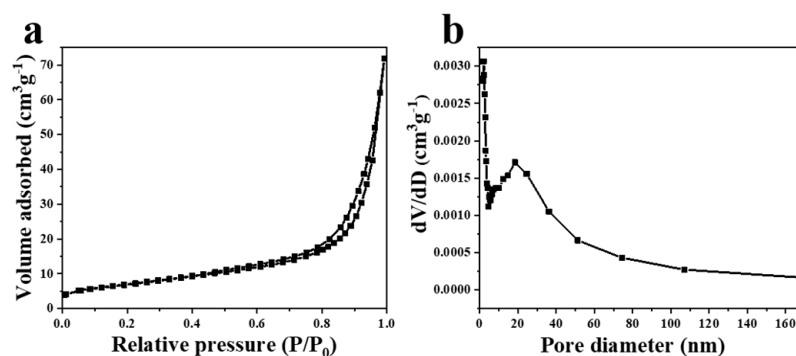


Figure 7. (a) N₂ adsorption-desorption isotherm of the GO/ZnO nanosheet composites, (b) the corresponding pore size distribution.

3.2. Sensing Performance

The electrical behavior of GO/ZnO nanosheet composites was investigated, and Figure S2 presents the corresponding current-voltage (I–V) curves. It can be seen that the almost linear characteristics of the ZnO/GO samples indicate the p-type ohmic contact of the sensing films.

The sensing performance of MOS sensors usually depends on the operating temperature. The responses of the GO/ZnO nanosheet composite sensor to 50 ppm n-propanol and isopropanol at different operating temperatures were investigated. As illustrated in Figure 8, the responses of GO/ZnO nanosheet composites to both n-propanol and isopropanol first increase with the increasing working temperature. However, when the temperature increases beyond 300 °C, the responses decrease. At low temperatures, there

are not enough O^{2-} anions on the surface of the GO/ZnO nanosheet composites to react with n-propanol and isopropanol molecules, and when the working temperature is too high, the desorption rate of molecules is far greater than the adsorption rate, thus resulting in a decrease in the response of the GO/ZnO nanosheet composites. Thus, the optimum operating temperature of the GO/ZnO nanosheet composites is 300 °C, and the subsequent gas-sensing tests were carried out at this temperature.

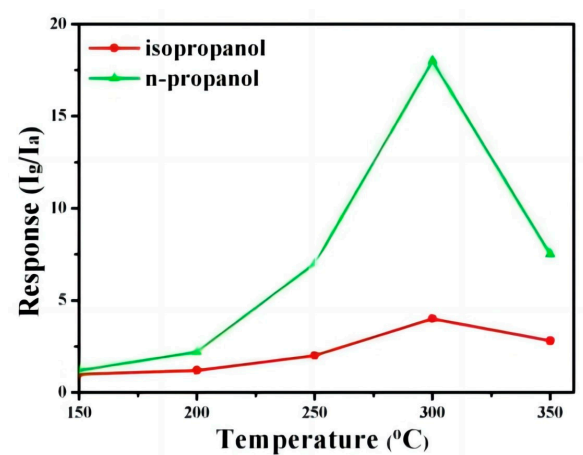


Figure 8. Responses of the GO/ZnO nanosheet composite sensor to 50 ppm isopropanol and n-propanol at different operating temperatures.

The real-time responses of the GO/ZnO nanosheet composites to n-propanol at different concentrations were also investigated, and the results are presented in Figure 9a. With an increase in the n-propanol concentration from 5 to 200 ppm, the response currents increase rapidly, and then immediately drop as the n-propanol gas is removed from the testing chamber. Figure 9b displays the plot of the sensitivity as a function of the concentration of n-propanol, revealing a linear range from 5 to 200 ppm. The least-squares fitting is $y = 5.48 + 0.26x$, and the regression coefficient (R^2) is 97.6%. The real-time response curves of GO/ZnO nanosheet composites to 50 ppm n-propanol and isopropanol at 300 °C are shown in Figure 10. The sensitivity of the GO/ZnO nanosheet composites to 50 ppm n-propanol and isopropanol is 17.2 and 4.4, respectively. In addition, the responses and recovery of the composites to both n-propanol and isopropanol are very fast, and the corresponding response times are 45 and 36 s, while the recovery times are 15 and 19 s, respectively. The results indicate that the GO/ZnO nanosheet composites have a good response to n-propanol.

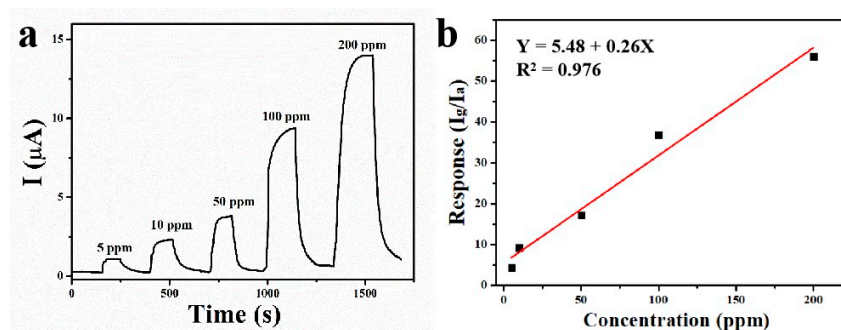


Figure 9. (a) Real-time responses of the GO/ZnO nanosheet composites to n-propanol at different concentrations at 300 °C, (b) the corresponding plots of the response vs. concentration.

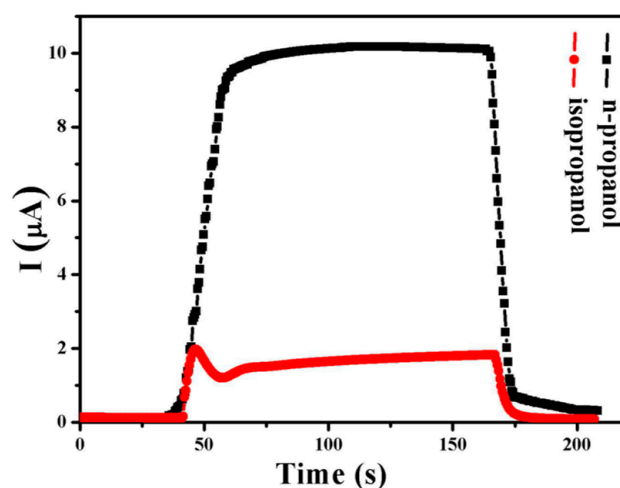


Figure 10. Real-time responses of GO/ZnO nanosheet composites to 50 ppm n-propanol and 50 ppm isopropanol at 300 °C.

The sensing performance of the GO/ZnO nanosheet composites was also compared with that of the porous ZnO nanosheets, and the results are presented in Figure 11. As shown, the responses of the ZnO nanosheets to 50 ppm n-propanol and isopropanol are 2.58 and 2.39, respectively. Nevertheless, when the ZnO nanosheets are coupled with GO nanosheets, the sensing performance of the composites is largely enhanced, especially to n-propanol. Obviously, this huge enhancement in sensing performance is due to the modification with GO.

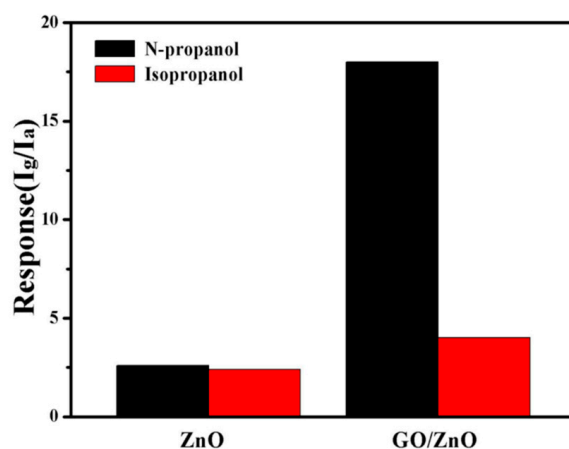


Figure 11. Response sensitivity of the porous ZnO nanosheets and GO/ZnO nanosheet composites to 50 ppm n-propanol and 50 ppm isopropanol at 300 °C.

The selectivity of the gas sensor is an important parameter for its application. Thus, the sensing properties of the GO/ZnO nanosheet composites to 50 ppm of methanol, ethanol, n-propanol, isopropanol, ammonia, methanal, benzene and hydrogen were investigated at 300 °C, and the results are presented in Figure 12. Obviously, the responses of the GO/ZnO nanosheet composites to ammonia, methanal and benzene are not high, namely 2.2, 1.5 and 1.2, respectively. For alcohols, the responses of the composites increase significantly. As well, the sensitivity of the GO/ZnO nanosheet composites largely increases with the growth of the carbon chain. The sensitivities of the GO/ZnO nanosheet composites to methanol, ethanol and n-propanol are 2.7, 7.0 and 17.2, respectively. Furthermore, the sensitivity of the composites to isopropanol, the isomer of n-propanol, largely reduces to 4.0. Thus, it is believed that the GO/ZnO nanosheet composites can identify n-propanol in a complex environment. The sensing performance of the GO/ZnO nanosheet composites was also compared with other values from the literature, and the results are presented in

Table 1. Obviously, the GO/ZnO nanosheet composites exhibit good sensitivity towards n-propanol.

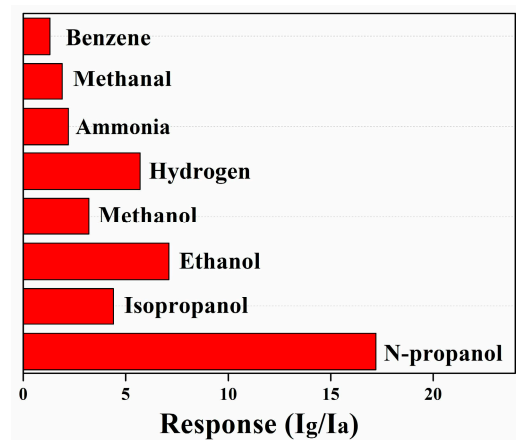


Figure 12. Responses of the GO-decorated porous single-crystalline ZnO nanosheets to 50 ppm of various gases at 300 °C.

Table 1. N-propanol sensors based on metal oxide nanostructures.

Sensing Materials	Temperature (°C)	Response @ Concentration (ppm)	Selectivity	Response Time (s)	References
ZnO nanowires	300	30.1@50 (2-propanol)	General	5	[33]
CuO nanofiber	200	4.66@100	General	4.66	[34]
TeO ₂ nanowires	50	3.15@500	Poor	20	[35]
CuO/CuCo ₂ O ₄ nanotubes	Room temperature	14@100	General	6.3	[36]
Cu ₂ O hollow microspheres	187	11@100	General	50	[37]
GO/ZnO nanosheet composites	300	17.2@50	Good	45	This work

The sensing mechanism of the GO/ZnO nanosheet composites was also deduced. As shown in Figure 13, GO nanosheets exhibit a p-type semiconductor behavior, while ZnO is an n-type semiconductor; thus, the p-n heterojunction of GO and ZnO is formed. When working, both of the GO and ZnO nanosheets are hot excited. As GO (4.5 eV) and ZnO (4.22 eV) have different work functions, the electrons in the higher energy level will be transferred to the lower energy level [21,26]. In the GO/ZnO heterojunction, the electrons will transfer from p-GO to n-ZnO, and the holes move in the opposite direction until equilibrium. The abundant oxygen vacancies and efficient electron mobility at the GO/ZnO heterojunction will provide more active sites for gas adsorption by increasing the specific surface area. Furthermore, they supply more channels to facilitate the diffusion of gas molecules, and consequently, favor the enhancement of n-propanol detection. Moreover, the unique structure of the ZnO nanosheet is also beneficial for the sensing properties of the composites. First, the porous structure provides more active sites. Due to the porous structure, there are more surface defects on the surface of the nanosheet, and those defects can effectively adsorb VOC molecules. In addition, these nanoholes could be the ideal transmission channel for the target gases, effectively facilitating the diffusion of gas molecules, which can greatly increase the sensing performance of the composite. Second, the single-crystalline structure of individual nanosheets can also increase the sensitivity. During transportation, electrons need not jump cross-grain boundaries, which is beneficial for the stability of the sensing materials. Third, the ZnO nanosheets are ultra-thin, which makes

the space charge layers cover the whole nanosheet. Fourth, in the composite, both ZnO and GO are lamellar structures, which grant the composite a larger boundary area; thus, electrons can be effectively transferred between the GO/ZnO nanosheets heterogeneously. Thus, the composites exhibit superior n-propanol sensing performance.

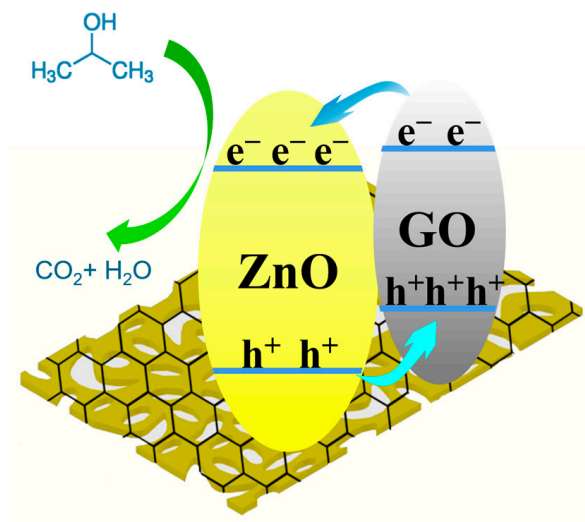


Figure 13. Sensing mechanism of the GO/ZnO nanosheet composites.

The stability of the GO/ZnO nanosheet composite sensor was further studied. As shown in Figure 14, there is no significant reduction in the response of the composite during a 14-day test. It is believed that the good stability of the GO/ZnO nanosheet composite can be attributed to the unique structure of the porous ZnO nanosheet.

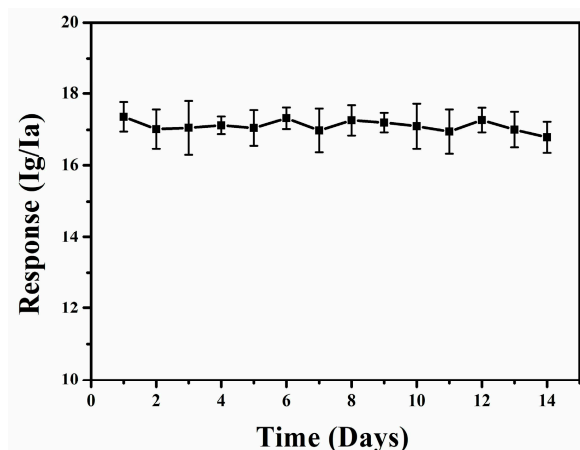


Figure 14. Response curve of the GO/ZnO nanosheet composites to 50 ppm n-propanol after 14 days of testing.

4. Conclusions

In conclusion, the GO/ZnO nanosheet composites were successfully synthesized through a hydrothermal method. In the composites, the ZnO nanosheets of hexagonal wurtzite are closely wrapped by GO lamellae, and the unique structure makes the GO/ZnO nanosheet composites exhibit a high response, excellent selectivity and stability in n-propanol detection. At the optimized temperature of 300 °C, the GO/ZnO nanosheet composites exhibit a linear response in n-propanol detection in a large range. Moreover, the sensing performance of the composites to n-propanol is largely higher than to other VOC gases, indicating a high sensitivity and selectivity in n-propanol detection. This can be ascribed to the higher electron-separation efficiency and larger depletion layer brought

by the modification of the GO on ZnO nanosheets. It is considered that the GO/ZnO nanosheet composites have a great application potential in n-propanol detection.

Supplementary Materials: The following supporting information can be downloaded at: <https://www.mdpi.com/article/10.3390/chemosensors11010065/s1>, Figure S1: The statistical distributions of the length and width of the GO/ZnO nanosheet composites; Figure S2: The corresponding current–voltage (I–V) curves of the GO/ZnO nanosheet composites.

Author Contributions: Conceptualization, J.L.; methodology, Y.C.; software, A.W.; validation, S.C. and D.W.; formal analysis, Z.J.; investigation, J.L.; writing—original draft preparation, J.L.; writing—review and editing, Q.Q.; supervision, Z.J.; funding acquisition, Z.J. All authors have read and agreed to the published version of the manuscript.

Funding: This research was funded by the National Key Research and Development (No. 2019YFC0408504), Natural Science Foundation of Anhui Province (No. 2008085MB44), Natural Science Research Project of Anhui Educational Committee (No. 2022AH040046, KJ2019A0772) and Young Talents and PhD Start-up Fund Project from Anhui Jianzhu University (2018QD52, 2019QDZ30).

Institutional Review Board Statement: Not applicable.

Informed Consent Statement: Not applicable.

Data Availability Statement: The data presented in this study are openly available.

Conflicts of Interest: We declare that we have no financial and personal relationships with other people or organizations that can inappropriately influence our work, and there is no professional or other personal interest of any nature or kind in any product, service and/or company that could be construed as influencing the position presented in, or the review of, the manuscript entitled.

References

1. Han, B.; Liu, X.; Xing, X.; Chen, N.; Xiao, X.; Liu, S.; Wang, Y. A high response butanol gas sensor based on ZnO hollow spheres. *Sensors Actuators Chem.* **2016**, *237*, 423–430. [[CrossRef](#)]
2. Meng, F.L.; Zheng, H.X.; Chang, Y.L.; Zhao, Y.; Li, M.Q.; Wang, C.; Sun, Y.F.; Liu, J., H. One-step synthesis of Au/SnO₂/RGO nanocomposites and their VOC sensing properties. *IEEE Trans. Nanotechnol.* **2018**, *172*, 212–219. [[CrossRef](#)]
3. Ma, A.; Park, H.J.; Seo, J.H.; Jang, K.Y.; Lee, H.K.; Kim, D.Y.; Lee, J.E.; Nam, K.M.; Lee, D.S. Phase transition of non-equilibrium wurtzite CoO: Spontaneous deposition of sensing material for ultrasensitive detection of acetone. *Sensors Actuators B Chem.* **2020**, *308*, 127698. [[CrossRef](#)]
4. Qin, W.B.; Yuan, Z.Y.; Gao, H.L.; Zhang, R.; Meng, F.L. Perovskite-structured LaCoO₃ modified ZnO gas sensor and investigation on its gas sensing mechanism by first principle. *Sens. Actuators B Chem.* **2021**, *341*, 130015. [[CrossRef](#)]
5. Ji, H.Y.; Qin, W.B.; Yuan, Z.Y.; Meng, F.L. Qualitative and quantitative recognition method of drug-producing chemicals based on SnO₂ gas sensor with dynamic measurement and PCA weak separation. *Sens. Actuators B Chem.* **2021**, *348*, 130698. [[CrossRef](#)]
6. Caicedo, N.; Leturcq, R.; Raskin, J.-P.; Flandre, D.; Lenoble, D. Detection mechanism in highly sensitive ZnO nanowires network gas sensors. *Sensors Actuators B Chem.* **2019**, *297*, 126602. [[CrossRef](#)]
7. Bhati, V.S.; Hojamberdiev, M.; Kumar, M. Enhanced sensing performance of ZnO nanostructures-based gas sensors: A review. *Energy Rep.* **2020**, *6*, 46–62. [[CrossRef](#)]
8. Wang, C.N.; Li, Y.L.; Gong, F.L.; Zhang, Y.H.; Fang, S.M.; Zhang, H.L. Advances in doped ZnO nanostructures for gas sensor. *Chem. Rec.* **2020**, *20*, 1553–1567. [[CrossRef](#)] [[PubMed](#)]
9. Meng, F.L.; Shi, X.; Yuan, Z.Y.; Ji, H.Y.; Qin, W.B.; Shen, Y.B.; Xing, C.Y. Detection of Four Alcohol Homologue Gases by ZnO Gas Sensor in Dynamic Interval Temperature Modulation Mode. *Sens. Actuators B Chem.* **2022**, *350*, 130867. [[CrossRef](#)]
10. Nundy, S.; Eom, T.Y.; Kang, J.G.; Suh, J.; Cho, M.; Park, J.S.; Lee, H.J. Flower-shaped ZnO nanomaterials for low-temperature operations in NO_x gas sensors. *Ceram. Int.* **2020**, *46*, 5706–5714. [[CrossRef](#)]
11. Alev, O.; Sarica, N.; Özdemir, O.; Arslan, L.C.; Büyükköse, S.; Öztürk, Z.Z. Cu-doped ZnO nanorods based QCM sensor for hazardous gases. *J. Alloy. Compd.* **2020**, *826*, 154177. [[CrossRef](#)]
12. Zhang, L.; Yin, M.; Qiu, J.; Qiu, T.; Chen, Y.; Qi, S.; Wei, X.; Tian, X.; Xu, D. Mesoporous ZnO nanosheet as gas sensor for sensitive triethylamine detection. *Anal. Bioanal. Chem.* **2022**, *414*, 2181–2188. [[CrossRef](#)] [[PubMed](#)]
13. Campos, A.C.; Paes, S.C.; Correa, B.S.; Cabrera-Pasca, G.A.; Costa, M.S.; Costa, C.S.; Otubo, L.; Carbonari, A.W. Growth of long ZnO nanowires with high density on the ZnO surface for gas sensors. *ACS Appl. Nano Mater.* **2019**, *3*, 175–185. [[CrossRef](#)]
14. Kim, J.W.; Porte, Y.; Ko, K.Y.; Kim, H.; Myoung, J.M. Micropatternable double-faced ZnO nanoflowers for flexible gas sensor. *ACS Appl. Mater. Inter.* **2017**, *9*, 32876–32886. [[CrossRef](#)]

15. Choi, S.M.; Kim, Y.M.; Mirzaei, A.; Kim, H.S.; Kim, S.I.; Baek, S.H.; Chun, D.W.; Jin, C.; Lee, H.K. Selective, sensitive, and stable NO₂ gas sensor based on porous ZnO nanosheets. *Appl. Surf. Sci.* **2021**, *568*, 150910. [[CrossRef](#)]
16. Liu, J.; Zhang, L.; Fan, J.; Zhu, B.; Yu, J. Triethylamine gas sensor based on Pt-functionalized hierarchical ZnO microspheres. *Sensors Actuators B Chem.* **2021**, *331*, 129425. [[CrossRef](#)]
17. Young, S.J.; Chu, Y.L. Platinum nanoparticle-decorated ZnO nanorods improved the performance of methanol gas sensor. *J. Electrochem. Soc.* **2020**, *167*, 147508. [[CrossRef](#)]
18. Aubekerov, K.K.; Punegov, N.; Sergeenko, R.; Kuznetsov, A.; Kondratev, V.M.; Kadinskaya, S.A.; Nalimova, S.S.; Moshnikov, V.A. Synthesis and study of gas sensitive ZnFe₂O₄-modified ZnO nanowires. *J. Phys.* **2022**, *2227*, 012014. [[CrossRef](#)]
19. Xu, X.-Y.; Yan, B. Eu(III)-functionalized ZnO@MOF heterostructures: Integration of pre-concentration and efficient charge transfer for the fabrication of a ppb-level sensing platform for volatile aldehyde gases in vehicles. *J. Mater. Chem. A* **2017**, *5*, 2215–2223. [[CrossRef](#)]
20. Ugale, A.D.; Umarji, G.G.; Jung, S.H.; Deshpande, N.G.; Lee, W.; Cho, H.K.; Yoo, J.B. ZnO decorated flexible and strong graphene fibers for sensing NO₂ and H₂S at room temperature. *Sensors Actuators B Chem.* **2020**, *308*, 127690. [[CrossRef](#)]
21. Zhang, J.; Jia, X.; Liu, T.; Yang, J.; Wang, S.; Li, Y.; Shao, D.; Feng, L.; Song, H. Facile strategy to synthesize porous GO/ZnO heterostructure for enhanced acetone gas sensing properties. *Sensors Actuators B Chem.* **2022**, *359*, 131601. [[CrossRef](#)]
22. Huang, W.C.; Tsai, H.J.; Lin, T.C.; Weng, W.C.; Chang, Y.C.; Chiu, J.L.; Lin, J.-J.; Lin, C.F.; Lin, Y.-S.; Chen, H. Incorporation of carbon nanotube and graphene in ZnO nanorods-based hydrogen gas sensor. *Ceram. Int.* **2018**, *44*, 12308–12314. [[CrossRef](#)]
23. Wu, J.; Shen, X.; Jiang, L.; Wang, K.; Chen, K. Solvothermal synthesis and characterization of sandwich-like graphene/ZnO nanocomposites. *Appl. Surf. Sci.* **2010**, *256*, 2826–2830. [[CrossRef](#)]
24. Khosravi, Y.; Sasar, M.; Abdi, Y. Light-induced oxygen sensing using ZnO/GO based gas sensor. *Mat. Sci. Semicon. Proc.* **2018**, *85*, 9–14. [[CrossRef](#)]
25. Galstyan, V.; Comini, E.; Kholmanov, I.; Faglia, G.; Sberveglieri, G. Reduced graphene oxide/ZnO nanocomposite for application in chemical gas sensors. *RSC Adv.* **2016**, *6*, 34225–34232. [[CrossRef](#)]
26. Kamble, C.; Narwade, S.; Mane, R. Detection of acetylene (C₂H₂) gas using Ag-modified ZnO/GO nanorods prepared by a hydrothermal synthesis. *Mat. Sci. Semicon. Proc.* **2023**, *153*, 107145. [[CrossRef](#)]
27. Vessalli, B.A.; Zito, C.A.; Perfecto, T.M.; Volanti, D.P.; Mazon, T. ZnO nanorods/graphene oxide sheets prepared by chemical bath deposition for volatile organic compounds detection. *J. Alloys Compd.* **2017**, *696*, 996–1003. [[CrossRef](#)]
28. Singh, G.; Choudhary, A.; Haranath, D.; Joshi, A.G.; Singh, N.; Singh, S.; Pasricha, R. ZnO decorated luminescent graphene as a potential gas sensor at room temperature. *Carbon* **2012**, *50*, 385–394. [[CrossRef](#)]
29. Yin, Y.; Shen, Y.; Zhou, P.; Lu, R.; Li, A.; Zhao, S.; Liu, W.; Wei, D.; Wei, K. Fabrication, characterization and n-propanol sensing properties of perovskite-type ZnSnO₃ nanospheres based gas sensor. *Appl. Surf. Sci.* **2020**, *509*, 145335. [[CrossRef](#)]
30. Mokoena, T.P.; Hillie, K.T.; Swart, H.C.; Leshabane, N.; Tshilongo, J.; Motaung, D.E. Fabrication of a propanol gas sensor using p-type nickel oxide nanostructures: The effect of ramping rate towards luminescence and gas sensing characteristics. *Mater. Chem. Phys.* **2020**, *253*, 123316. [[CrossRef](#)]
31. Dai, K.; Lu, L.H.; Liang, C.H.; Dai, J.M.; Zhu, G.P.; Liu, Z.L.; Liu, Q.Z.; Zhang, Y.X. Graphene oxide modified ZnO nanorods hybrid with high reusable photocatalytic activity under UV-LED irradiation. *Mater. Chem. Phys.* **2014**, *143*, 1410–1416. [[CrossRef](#)]
32. Jin, Z.; Zhang, Y.X.; Meng, F.L.; Jia, Y.; Luo, T.; Yu, X.Y.; Wang, J.; Liu, J.H.; Huang, X.J. Facile synthesis of porous single crystalline ZnO nanoplates and their application in photocatalytic reduction of Cr(VI) in the presence of phenol. *J. Hazard. Mater.* **2014**, *276*, 400–407. [[CrossRef](#)] [[PubMed](#)]
33. Huang, J.R.; Ren, H.B.; Sun, P.P.; Gu, C.P.; Sun, Y.F.; Liu, J.H. Facile synthesis of porous ZnO nanowires consisting of ordered nanocrystallites and their enhanced gas-sensing. *Sensors Actuators B Chem.* **2013**, *188*, 249–256. [[CrossRef](#)]
34. Dong, C.J.; Xing, X.X.; Chen, N.; Liu, X.; Wang, Y.D. Biomimetic synthesis of hollow CuO fibers for low-ppm-level n-propanol detection via a facile solution combustion method. *Sensors Actuators B Chem.* **2016**, *230*, 1–8.
35. Shen, Y.B.; Fan, A.F.; Wei, D.Z.; Gao, S.L.; Liu, W.G.; Han, C.; Cui, B.Y. A low-temperature n-propanol gas sensor based on TeO₂ nanowires as the sensing layer. *RSC Adv.* **2015**, *5*, 29126. [[CrossRef](#)]
36. Alali, K.T.; Lu, Z.T.; Zhang, H.S.; Liu, J.Y.; Liu, Q.; Li, R.M.; Aljebawi, K.; Wang, J. P-p heterojunction CuO/CuCo₂O₄ nanotubes synthesized via electrospinning technology for detecting n-propanol gas at room temperature. *Inorg. Chem. Front.* **2017**, *4*, 1219–1230. [[CrossRef](#)]
37. Wang, N.; Zhou, Y.; Chen, K.; Wang, T.S.; Sun, P.; Wang, C.G.; Chuai, X.H.; Zhang, S.M.; Liu, X.M.; Lu, G.Y. Double shell Cu₂O hollow microspheres as sensing material for high performance n-propanol sensor. *Sensors Actuators B Chem.* **2021**, *333*, 129540. [[CrossRef](#)]

Disclaimer/Publisher's Note: The statements, opinions and data contained in all publications are solely those of the individual author(s) and contributor(s) and not of MDPI and/or the editor(s). MDPI and/or the editor(s) disclaim responsibility for any injury to people or property resulting from any ideas, methods, instructions or products referred to in the content.